3-DIMENSIONAL FINITE ELEMENT MODELING OF SELECTIVE LASER MELTING TI-6AL-4V ALLOY

C.H. Fu, Y.B. Guo[*]

Dept. of Mechanical Engineering, The University of Alabama, Tuscaloosa, AL 35487, USA

REVIEWED

Abstract

Selective laser melting (SLM) is widely used in making three-dimensional functional parts layer by layer. Temperature magnitude and history during SLM directly determine the molten pool dimensions and surface integrity. However, due to the transient nature and small size of the molten pool, the temperature gradient and the molten pool size are very challenging to measure and control. A 3-dimensional finite element simulation model has been developed to simulate multi-layer deposition of Ti-6Al-4V in SLM. A physics-based layer build-up approach coupled with a surface moving heat flux was incorporated into the modeling process. The melting pool shape and dimensions were predicted and experimentally validated. Temperature gradient and thermal history in the multi-layer build-up process was also obtained. Furthermore, the influences of process parameters and materials on the melting process were evaluated.

1. Introduction

1.1. Selective laser melting (SLM)

Layer manufacturing (LM) has been developed for over 20 years. It is widely used in making three-dimensional parts directly from CAD models by adding material layer by layer, rather than removing material. Rapid manufacturing (RM), as a layer manufacturing process, is aiming at producing functional parts that can be directly used as end-use products rather than prototypes. The advantages of RM include: (1) it allows fabrication of geometrically complex parts, even for parts that not possible to fabricate with subtractive manufacturing processes [1] and (2) it is a cost-effective process for single parts and small batches. The current challenge for RM is that it should guarantee long-term consistent components that have required physical, mechanical, and geometrical properties [2].

Selective laser melting (SLM) is a typical powder-based RM processes. SLM features fully melting of powder, thus near full density parts can be produced. The advantage of SLM over electron beam melting (EBM) and laser metal deposition (LMD) is that the equipment is relatively less complex. There is no need for high vacuum chamber to guide electron beam as opposed to EBM. There is also no stringent alignment needed between powder feeding nozzle and laser beam (as opposed to LMD) [3]. SLM is widely used in aerospace, automotive, biomedical, and energy industries [4-8].

[*] Corresponding author. Tel.: +1 205 348 2615; Fax: +1 205 348 6419.
  E-mail address: yguo@eng.ua.edu (Y.B. Guo).

Even though SLM is a very promising technique, due to the intense heat input, problems such as balling effect, deteriorated surface finish, tensile residual stress, and part distortion are still frequently observed in SLM process.

1.2. Process characteristics

Fig. 1(a) shows the schematic of SLM process. It uses a fine powder system to distribute a 20-100 μm layer onto the substrate plate inside a chamber containing inert gas. Then the layer is fused by selectively scan laser beam on the powder surface. The intensive laser energy fully melts the metal powders to form a solid metal. This process is repeated layer after layer until the part is complete.
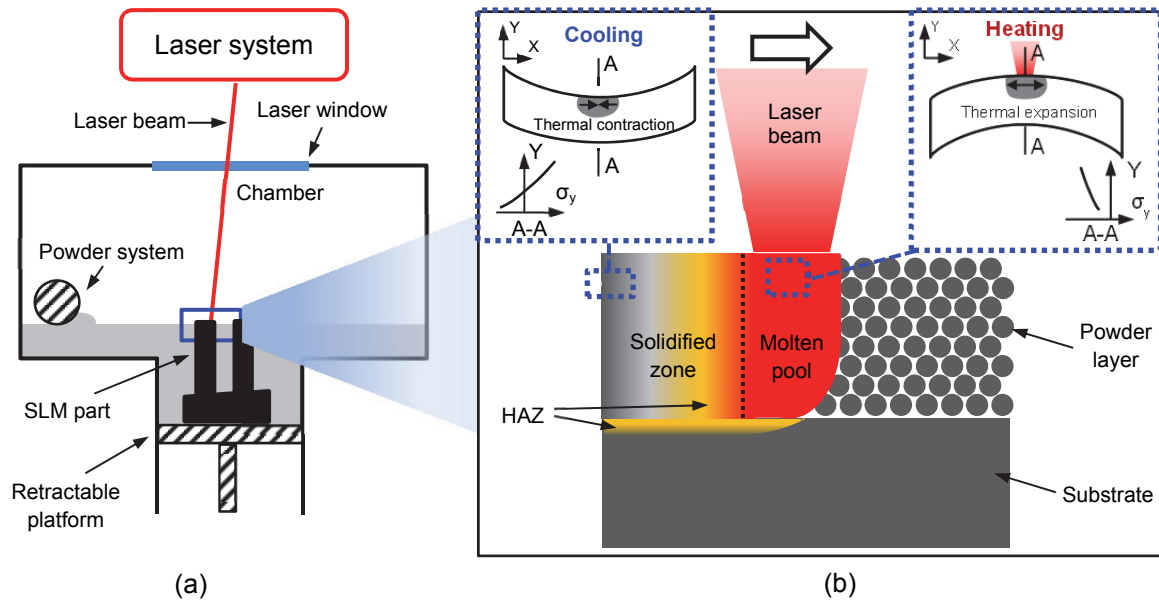

Fig. 1 Selective laser melting experimental setup and process principle.

The process principle of SLM is shown in Fig. 1(b), when laser beam scans on the powder surface, energy is transferred from the top surface to subsurface through various physical phenomena, such as absorption and scattering of the laser radiation, heat transfer, fluid flow within the molten pool, melting/evaporation, and chemical reactions.

Powder melting happens when the temperature reaches the material melting temperature. The dimension of the molten pool is greatly affected by the average applied energy per unit volume, which is mainly controlled by process parameters including laser power and scanning speed. It has been reported that higher scanning speed leads to an increasing length to diameter ratio in a molten pool. Such a molten pool with length to diameter ratio greater than π will cause balling effect [9]. The balling effect can be characterized by the break-up of the molten pool into balls, which degrades surface integrity of the final components. Therefore, to achieve the optimal surface integrity, the range of the optimal scanning speed is limited by the balling effect. It has also been reported that a higher laser power can expand the range for the optimal speed [10].

The nature of laser heating of a powder layer is considerably different from laser heating of a solid bulk body because of two reasons. First, laser absorptivity for powder layers is substantially higher than that of the bulk body due to their different granulomorphometry and density [10,11].

Second, thermal conductivity of powder bed is much lower than that of the opaque body since powder particles have limited contact area with each other, thus, heat transfer is only dominated by the low thermal conductivity of gas [12]. Due to these dissimilarities, it can be inferred that changing powder diameters and compactness can significantly affect heat conduction property during SLM.

In a SLM process, a very steep temperature gradient is generated due to the rapid heating of the upper surface by laser and slow heat conduction of underlying layers [9]. Temperature gradient induced surface tension gradient in the molten pool can cause convective motions, known as the Marangoni flow. Temperature gradients also induce high internal stresses. As shown in Fig. 1(b), when laser beam hits the top surface, the expansion of the heated layer is restricted by the vicinity area, therefore, a compressive stress is generated on the top surface. When the yield stress of the material is reached, plastic distortion occurs. As the laser moves away, cooling takes place; the contraction of the top layer is then restricted by the surrounding area, leading to a tensile residual stress on the top surface. The tensile residual stress will accumulate during each laser scan, which can cause delamination or cracks. Also, the cooling and shrinkage will create shorter top layers than the bottom layers, thus, the component is distorted by bending towards the laser beam.

Products are formed from the consolidated material in SLM process. The temperature gradient controls the formation, motion, and rapid solidification of the molten pool, which directly determines the microstructure, material properties, and final surface integrity of the components. It was found that the material processed by SLM exhibit a very fine, non-equilibrium microstructure [13]. However, the excessive heat input will elongate the grains and induce an heat affected zone (HAZ), which will degrade the material property and performance.

The temperature gradient mechanism is critical for SLM due to the following reasons: it directly controls the dimension and stability of a molten pool, which plays a large role in determining surface roughness and porosity of the parts. Temperature gradient also controls the formation of the HAZ, tensile stresses, and part distortion. If temperature gradient can be accurately measured and controlled, surface integrity and functionality of the final parts can be significantly improved. However, the temperature gradient is very challenging to measure due to its very small size and transient nature. Therefore, a finite element simulation was used in this study to gain insight into the process mechanism. The goal of this study is to understand the fundamental temperature gradient mechanism by developing a finite element model.

1.3. Literature review on SLM simulation

A few research has been conducted to simulate an SLM process to predict temperature gradient, stress formation, and part distortion. A successful finite element model of SLM needs to consider four coherent aspects: (1) a thermal model representing scanning laser thermal input, (2) a material model to define the temperature-dependent material property in the cyclic heat and cooling environment, (3) a physics-based method to describe the layer build-up process, and (4) a laser material interaction model that accounts for the transient thermomechanical phenomena.

A thermal model with spatial accuracy is critical to simulate the laser heating in SLM. The most commonly used heat flux model has the Gaussian form of

$$I = \frac{AP}{\pi r_0^2} \exp[-B \left(\frac{r}{r_0}\right)^2] \tag{1}$$

where I is the laser intensity, A is the laser absorption coefficient, P is the laser power, r_0 is the laser spot radius, B is the shape factor of the Gaussian distributed heat flux (typical value is 2), and r is the distance to laser beam center. Representative heat flux models that used in laser melting applications with different features are summarized in Table 1. Most previous works used surface heat flux rather than volumetric heat flux due to the very small layer thickness (30-100 μm) of powders.

Table 1: Representative Heat Flux Models

Heat Flux Types	Heat Flux Equations	Notes	Ref.
Surface (2D) heat flux	$q(r) = \dfrac{2P}{\pi r_0{}^2}\exp(-2\dfrac{r^2}{r_0{}^2})$	2D Gaussian distribution of surface heat flux	[14]
	$I(r,w) = \dfrac{2AP}{\pi w^2}\exp(-\dfrac{2r^2}{w^2})$	2D Gaussian distribution of surface intensity; absorptivity and characteristic radius included	[15,16]
	$q(r) = \dfrac{4.55P}{\pi R^2}\exp(-4.5\dfrac{r^2}{R^2})$	A different shape of Gaussian distribution was used	[17]
Volumetric (3D) heat flux	$f_{laser} = \dfrac{A \times I_0(x,y)}{\delta} \times \exp\left(-\dfrac{\left|z - z_{surface}\right|}{\delta}\right)$	Optical penetration depth was considered.	[18]

Beside an accurate thermal model, an effective material model that takes into account of the property change in the cyclic heating and cooling environment is also essential. It has been proved that thermophysical properties such as thermal conductivity and specific heat change significantly when material is heated up to liquid phase from solid phase [19]. Moreover, the thermal conductivity for solid substrate and powder bed are also significantly different. The effective thermal conductivity of loose metallic powders is controlled by gas in the pores, and it was found that for powders of 10-50 μm diameter, the effective thermal conductivity is typically from 0.1-0.2 W/mK. However, the thermal conductivity starts to rise sharply when the material starts to melt. Therefore, it is critical to include these property changes in SLM simulation.

To simulate the layer build-up process in SLM, Ding et al. [20] used multiple sequential steps in the simulation. More specifically, after each scan, the temperature from the previous step was imported into the next step for newly added layers. Another technique is to use the element "birth and death". The deposition of powder material on the powder bed to create a solid is analogous to the activation of new elements at desired time point [14]. Dai et al. [21] simulated the layer build-up process in SLM by adding all the elements within one layer simultaneously onto the previous layer. After adding the entire layer of the powder elements, the heat flux was applied on this newly added layer to simulate the laser thermal processing.

Although these simulation studies have explored the simulation of SLM process on different materials using different thermal modeling and element "death/birth" methods, little research has been done on a systematic finite element simulation of SLM including a moving surface heat flux, realistic layer build-up, and temperature-dependent multi-phases material properties. SLM is a very complex process with wide arrange of transient non-equilibrium phenomena taking place. Not only laser parameters, such as laser power or laser spot size, but also the material

properties such as temperature-dependent thermal properties play an important role in determining temperature gradient mechanism and molten pool behavior. Therefore, the objectives of this study are to: (1) develop a 3-dimensional finite element simulation model of SLM with an emphasis on a physics-based layer build-up approach coupled with a surface moving heat flux, (2) predict molten pool shape and dimensions with experimental validation, (3) study the effect of process parameters and materials on the melting process, and (4) gain insights into the temperature gradient mechanism of SLM process.

2. Simulation Approach

2.1. Model description

The finite element analysis (FEA) package Abaqus/Standard was used to incorporate both the moving heat flux subroutine and material properties to simulate the laser-material interaction in SLM. The mesh design is shown in Fig. 2. The workpiece is divided into two sections: substrate and powder layers. The dimensions of the substrate are 4 mm (length) × 1 mm (width) × 0.5 mm (thickness). The dimensions of the powder layer are 2 mm (length) × 0.2 mm (width) × 0.15 mm (thickness). The layer thickness is 30 μm and five layers are built-up in the simulation. The laser scanning direction is along the X-axis. Element size is biased with a higher density in the powder layers and top of the substrate. Within the fine mesh, the element size is 10 μm (length) × 5 μm (width) × 5 μm (thickness). The boundary condition on the bottom plane is fixed to provide proper constraint of the workpiece. Also, the model is symmetric with respect to X-Z plane so that only half of the workpiece needs to be modeled to decrease the computational time. The initial temperature is set to room temperature (20 °C).

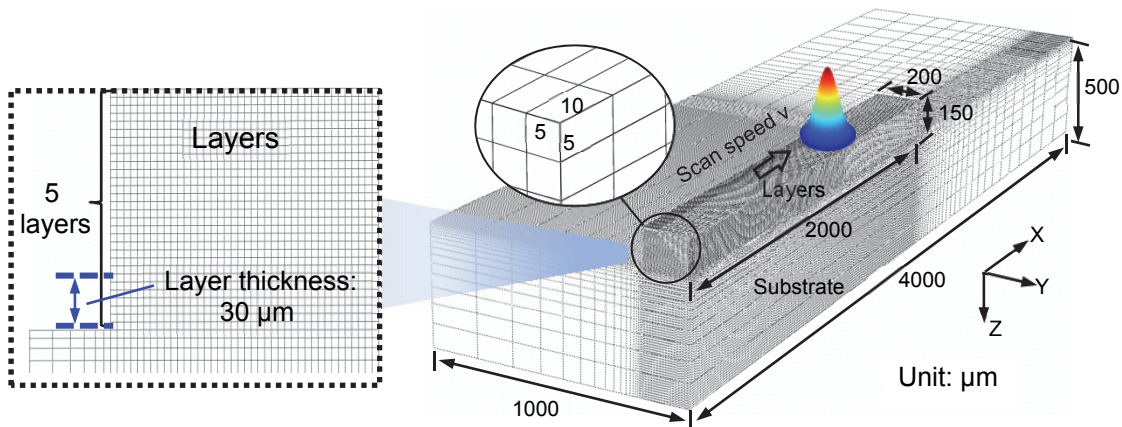

Fig. 2 Simulation schematic of SLM.

The simulation was performed using Abaqus/Standard since the moving heat flux subroutine DFLUX can be programed with the implicit solver. Another advantage of using the implicit solver is that the temporal discretization is more stable despite a certain reduction in computational efficiency.

1133

2.2. Modeling of surface moving heat flux

To simulate the characteristics of the heat flux of laser, a DFLUX user subroutine of surface heat flux was developed. The output of the subroutine was the heat flux given by the following equation:

$$F = \frac{AP}{\pi r^2} e^{\left(-2\frac{x^2+y^2}{r^2}\right)} \tag{2}$$

where F is the applied heat flux, A is the energy absorption coefficient, P is the laser power, and r is the laser spot radius on the top surface. Fig. 3 shows the Gaussian distribution of the heat flux at given conditions. As the laser power rises from 20 W to 80 W, the heat flux magnitude increases from 6 GW/m² to 30 GW/m², respectively.
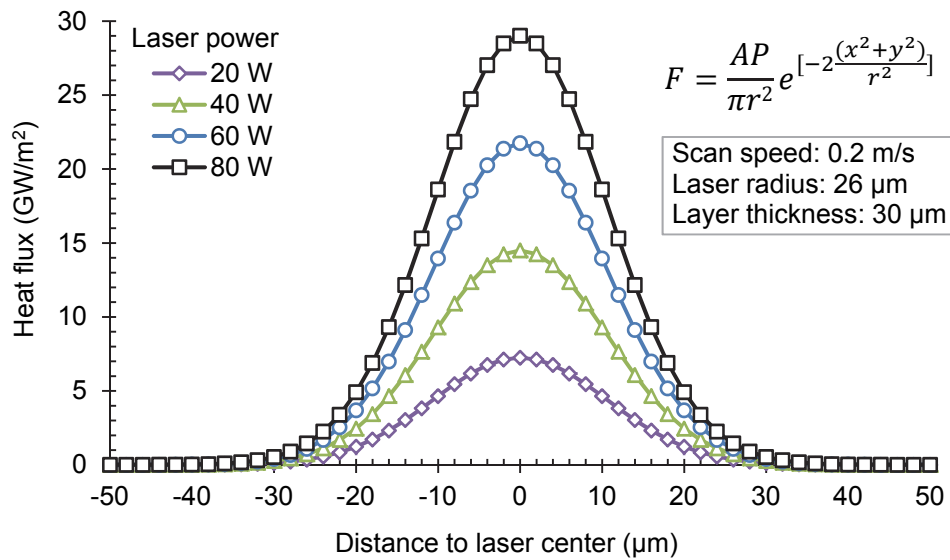

Fig. 3 Heat flux magnitude for 4 simulation cases.

2.3. Modeling of layer build-up

The layer build-up was modeled by the following three steps: First, the mesh of powder layers and substrate of the final SLM part is created. Second, all the elements within the powder layers are deactivated at the beginning of the analysis. Last, the elements in the first powder layer are activated followed by the first laser scan. This process is repeated for the successive layers so that a very close approximation of the actual SLM process can be simulated, where powders are laid layer by layer after each scan. Since the powder layer thickness is 30 μm in simulation and each powder layer contains 5 layers of elements for high mesh resolution, there are 48,000 elements for each powder layer. The powder depth in the experiment is the same as the powder layer thickness in simulation. A schematic of the layer build-up process is shown in Fig. 4.
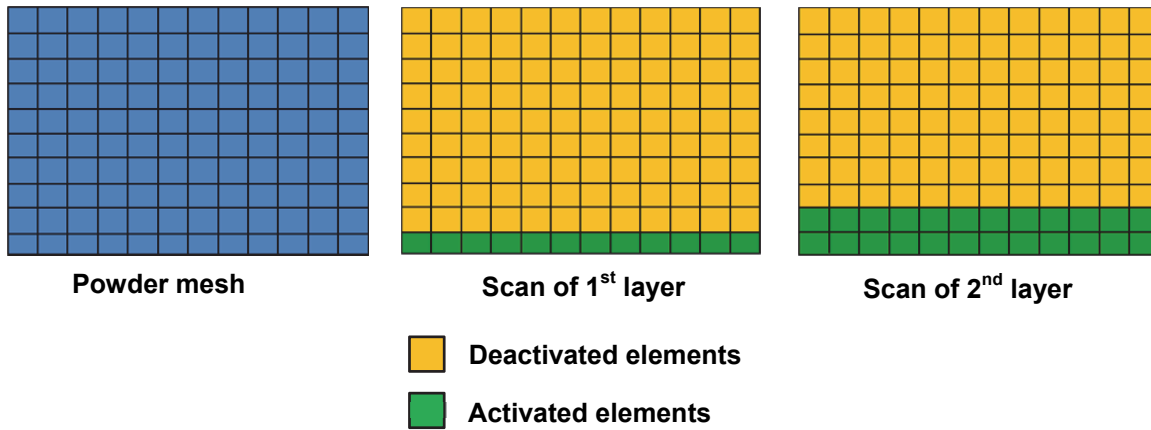
Powder mesh **Scan of 1ˢᵗ layer** **Scan of 2ⁿᵈ layer**

Deactivated elements

Activated elements

Fig. 4 Schematic of layer build-up process.

2.4. Material properties

Ti-6Al-4V was used in this study since it is widely used in SLM for aerospace and biomedical applications. The temperature-dependent material thermal properties of Ti-6Al-4V powder and substrate are listed in Table 2. In addition to the thermal properties, mechanical and physical properties including density, yield strength, elastic modulus, Poisson's ratio, melting/evaporation point, and latent heat were also considered (Table 3).

Table 2: Temperature Dependent Thermal Properties of Ti-6Al-4V [19,22,23]

Ti-6Al-4V Solid & Powder		Ti-6Al-4V Solid		Ti-6Al-4V Powder	
Specific heat	Temperature	Conductivity	Temperature	Conductivity	Temperature
J/kg·K	^{o}C	W/m·K	^{o}C	W/m·K	^{o}C
580	20	7.20	26.85	0.2	20
610	205	8.15	100.00	19.4	1605
670	425	9.44	200.00	28.3	1655
760	650	13.32	500.00		
930	870	18.20	876.85		
936	1000	19.79	1000.00		
1016	1200	26.26	1500.00		
1095	1400	28.27	1655.00		
1126	1655	37.00	2126.00		
		42.00	2426.85		

Table 3: Mechanical and Physical Properties of Ti-6Al-4V [23]

Density (Kg/m^3)	4428
Yield strength (MPa)	825
Elastic modulus (GPa)	110
Poisson's ratio	0.41
Melting point (^{o}C)	1655
Evaporation point (^{o}C)	2976
Solidus temperature (^{o}C)	1605
Liquidus temperature (^{o}C)	1655
Latent heat (J/Kg)	365000

2.5. Simulation conditions

The simulations were a sensitivity analysis to determine the effects of laser power on molten pool geometry and temperature gradient. The effect of material property, powder vs. solid, was also studied. Two different material properties were used for the elements in the build-up layers. In the first set of simulations, the powder properties with a low thermal conductivity were used, while the solid properties with a high thermal conductivity were used in the second set of simulations. This approach would provide insights of the effect of powder compactness on the pool geometry and temperature gradient mechanism.

The laser in this study is a continuous Nd:YAG laser (wavelength = 1.06 μm) that is widely used in actual SLM process. At this wavelength, the absorption coefficient for Ti-6Al-4V powder was assumed to be the same as pure titanium powder, which is equal to 0.77 [11]. The laser scanning speed is 0.2 m/s. The laser spot radius is 26 μm and the layer thickness is 30 μm for all the simulation cases.

3. Model Validation and Discussions

Fig. 5(a) shows the representative temperature contour when laser was scanning on the top layer. The molten pool dimension is indicated by the gray region, where the elements within this space have a temperature above the melting temperature of Ti-6Al-4V. A "comet tail" profile can be seen in Fig. 5(b). This asymmetry can be attributed to the movement of the laser as well as the fact that the heated-up material has greater conductivity than the untreated powder in front of the laser. This skewed temperature distribution towards the rear of the laser was also reported in other studies [14,16].
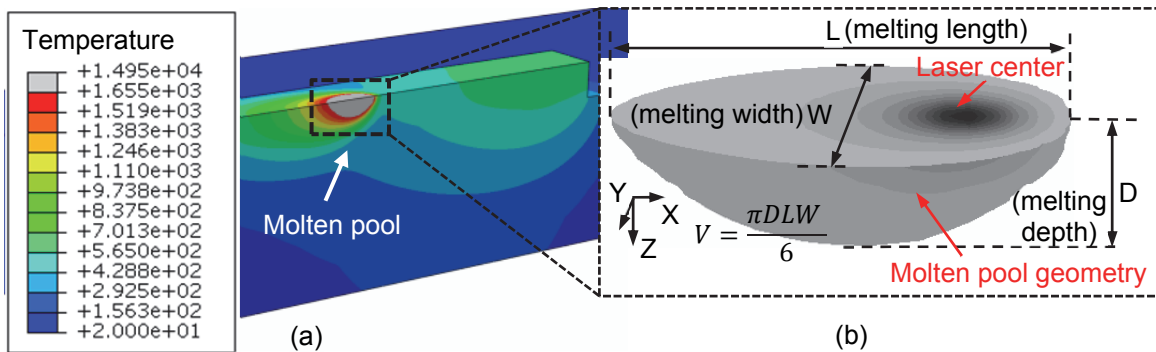

Fig. 5 (a) Representative temperature contour and (b) molten pool geometry.

3.1. Molten pool geometry and dimensions

Melting depth: The remelting depth for each layer has proven to be critical to microstructure evolution [13], remove contaminants [24], and prevent balling effect [10]. Therefore, it is important to monitor, predict, and control the melting depth for each layer during SLM.

Fig. 6 shows the effect of laser power on melting depth. It can be seen that as the laser power increased from 20 W to 80 W, the predicted melting depth increased from 20 μm to 40 μm, which is larger than the powder layer thickness. Remelting started to happen at laser power of 40 W. Moreover, as illustrated by the error bar, the predicted melting depth for all the five layers at the same laser power were very close, which indicates that the preheating of the previous layers had little influence on remelting of the subsequent layers at the concerned conditions.
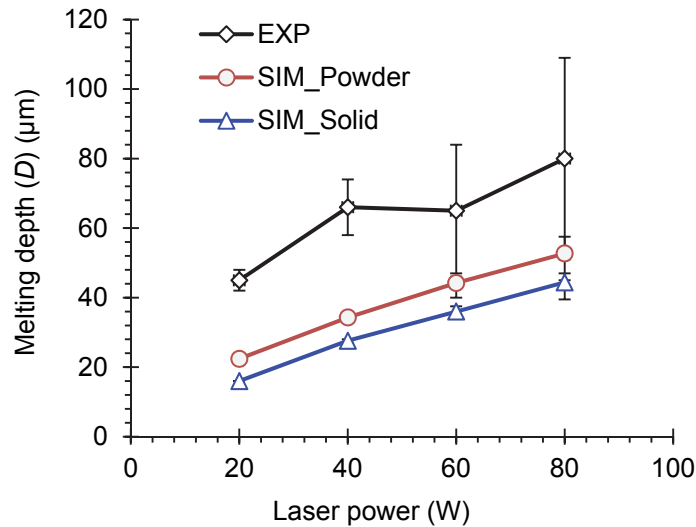
Fig. 6 Effect of laser power on melting depth.

To validate the simulation results, the predicted melting depths were compared with the experimental data at same SLM conditions [22]. The SLM experiments were conducted with a powder layer thickness of 30 μm by building a single track on a solid substrate. For comparison purpose, the simulation conditions are same as the experimental conditions. The predicted width and depth of molten pool were analyzed by optical microscopy based on the solidified microstructure. It can be seen that the predicted data agreed with the experimental data with in trend. The measured melting depths in experiments were higher than the predicted ones. The assumptions and error sources responsible for the discrepancies are as follows: (1) the absorptivity, specific heat, and thermal conductivity of the powder bed were obtained from the literature, which may be different from the actual values since these properties are greatly affected by powder size, compactness, and surrounding environment; (2) there may be uncertainties in experimental inputs that differentiate the experimental conditions with simulation, e.g., the laser power loss during delivery, laser spot size change due to defocus etc.; (3) there are measurement errors as indicated by the large size of the error bars. In addition, the experimental measurements were based on the solidified microstructure, where the microstructural boundaries are often difficult to characterize and could induce high non-uniformity and randomness in the measurement. These compounding factors influence the predictive accuracy of the simulation approach, which can be improved in the future.

Melting length/width: The predicted melting width is shown in Fig. 7. The predicted melting depth agreed with the experimental data in trend. As the laser power increased, the melting width almost increases linearly. The predicted melting length is shown in Fig. 8. For all the cases, the predicted length to width ratio is near 1.3, which is smaller than the critical value of π for balling effect [9]. This indicates that there was no balling effect at concerned conditions.
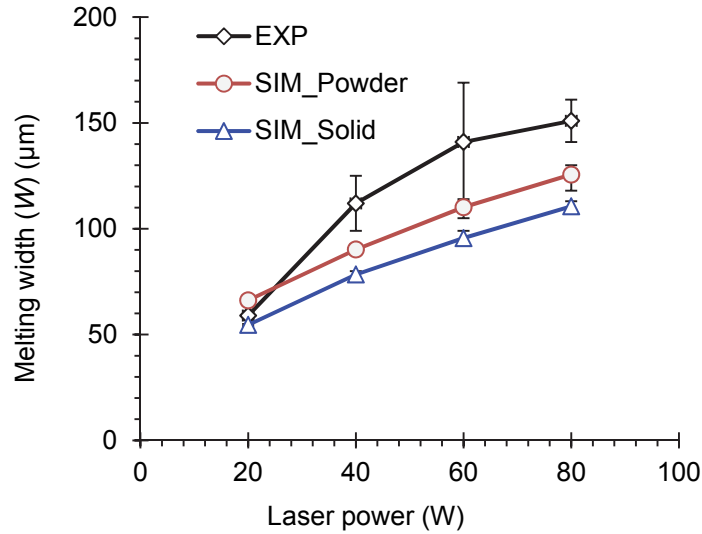

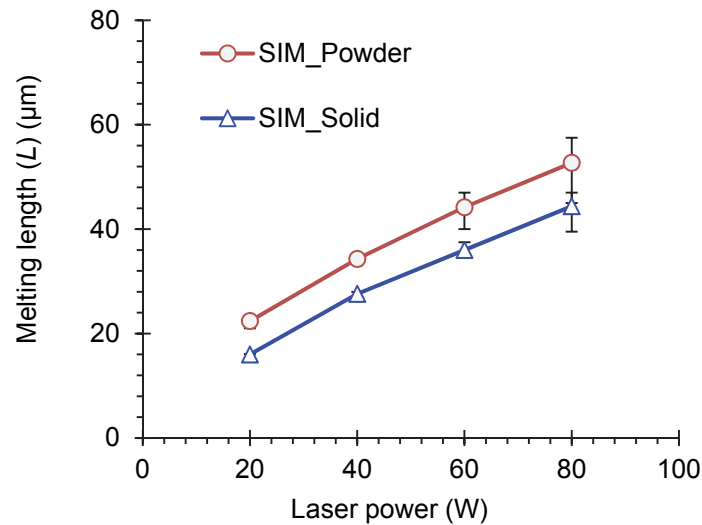Fig. 7 Effect of laser power on melting width.

Fig. 8 Effect of laser power on melting length.

Molten pool volume: It can be seen in Fig. 5 that the molten pool was in a near ellipsoid shape, and the volume of the molten pool can be approximated by

$$V = \frac{\pi DLW}{6} \tag{3}$$

1138

where D is the melting depth, L is the melting length, W is the melting width of the molten pool, respectively. As indicated in Fig. 9, when laser power increased, the molten pool volume increased dramatically.
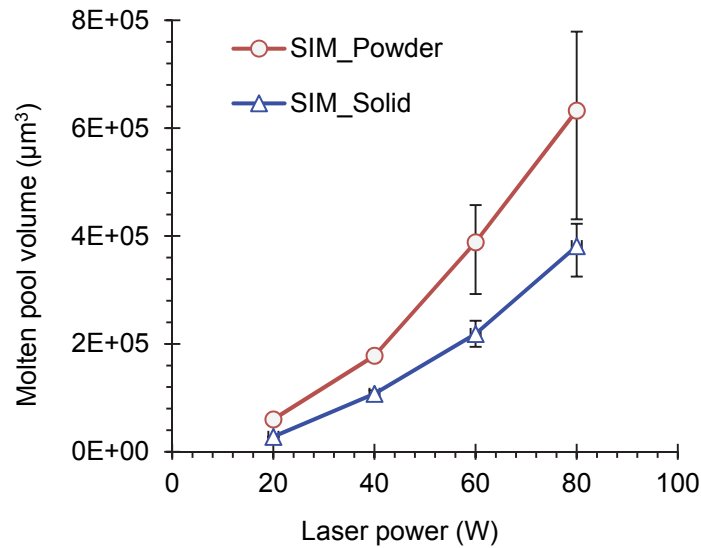

Fig. 9 Effect of laser power on molten pool volume.

The effect of material property: The changes of the molten pool depth, width, and volume were also plotted in Figs. 6-9. It can be observed that by using the solid property (higher thermal conductivity) in powder layers, the molten pool depth, width, length, and volume decreased. This finding suggests that the higher thermal conductivity of the solid "delivered" the thermal energy into the deeper and further vicinity, thus steep temperature gradient caused by the very low thermal conductivity of the powder was reduced. Therefore, it can be inferred that by using a more compact powders, steep temperature gradient can be reduced and the molten pool size can be decreased.

3.2. Temperature gradient
Depth direction: Temperature distributions in the subsurface are shown in Fig. 10. The temperatures decrease dramatically from the laser beam's center to the subsurface. At a laser power of 20 W, the temperature difference within 100 μm was smaller when compared to other 3 simulation cases (40 W, 60 W, and 80 W). As the laser power increases, temperature gradient becomes steeper. In addition, within 40 μm depth, the temperature distribution was significantly different for the concerned simulation cases. Beyond 40 μm, the temperature distribution for the simulated cases shared similar magnitude. This was due of the fact that at higher laser powers, more thermal energy was accumulated near the top surface due to the low thermal conductivity. Also, extreme high temperature was observed at the simulated conditions, this is non-practical since material would evaporate at such high temperatures.
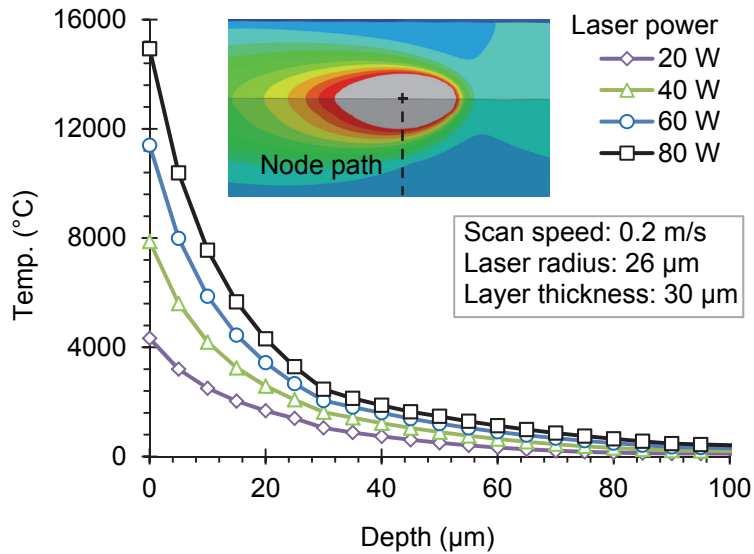
Fig. 10 Temperature gradient in layer depth direction.

Width direction: Temperature distributions in width direction are shown in Fig. 11. The temperatures decrease with the increased width. Also, it can be observed that the temperature distributions share a similar Gaussian distribution as the applied heat flux.
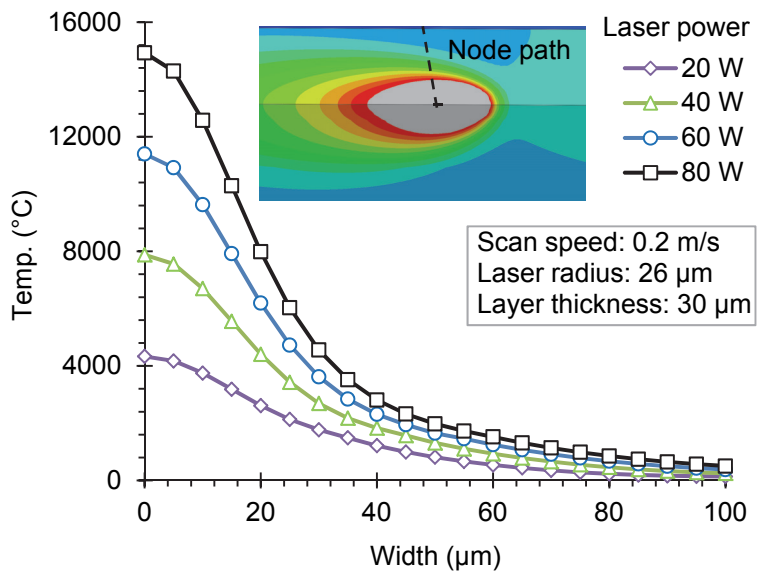

Fig. 11 Temperature gradient in layer width direction.

Laser scanning direction: Temperature distributions in the laser scanning direction are shown in Fig. 12. The temperatures decrease as moving away from the laser beam's center along the scanning direction. When compare the temperature gradients in depth, width, and laser scanning direction, it can be observed that the temperature gradient was much steeper in the depth direction. It is due to that the thermal conduction of powders in depth direction was

constrained by the thermal conductivity rather than the direct laser radiation in the width and laser scanning directions.
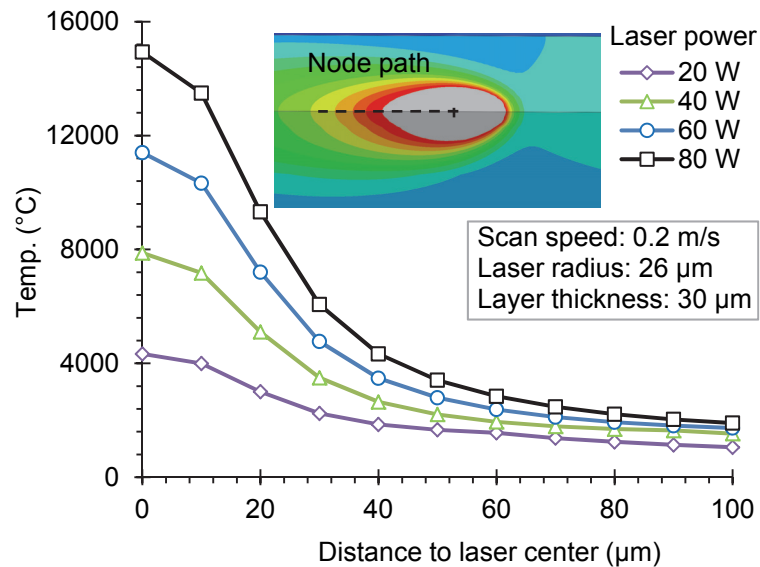

Fig. 12 Temperature gradient in laser scanning direction.

Thermal history: The thermal history at the selected location is shown in Fig. 13. The selected point was located on the top surface and in the middle of the first layer. The peak temperatures represent the start of each heating-cooling cycle during each laser scan. As seen in the figure, the material point experiences five heating-cooling cycles. At the lowest laser power (20 W), the 1st layer was raised above its melting temperature only once during the first laser scan, while at the highest laser power (80 W), the 1st layer was melted 3 times. As more layers were deposited in the 4th and 5th laser scan, the temperature drops below the melting temperature. This suggests that addition of layers and subsequent scanning are of great importance to the previous layers. It can be further noticed that cooling to the ambient temperature after each laser scan occurred only within a few milliseconds, which indicating the material was subjected to rapid heating-cooling cycles, which leads to very high tensile residual stresses [25].
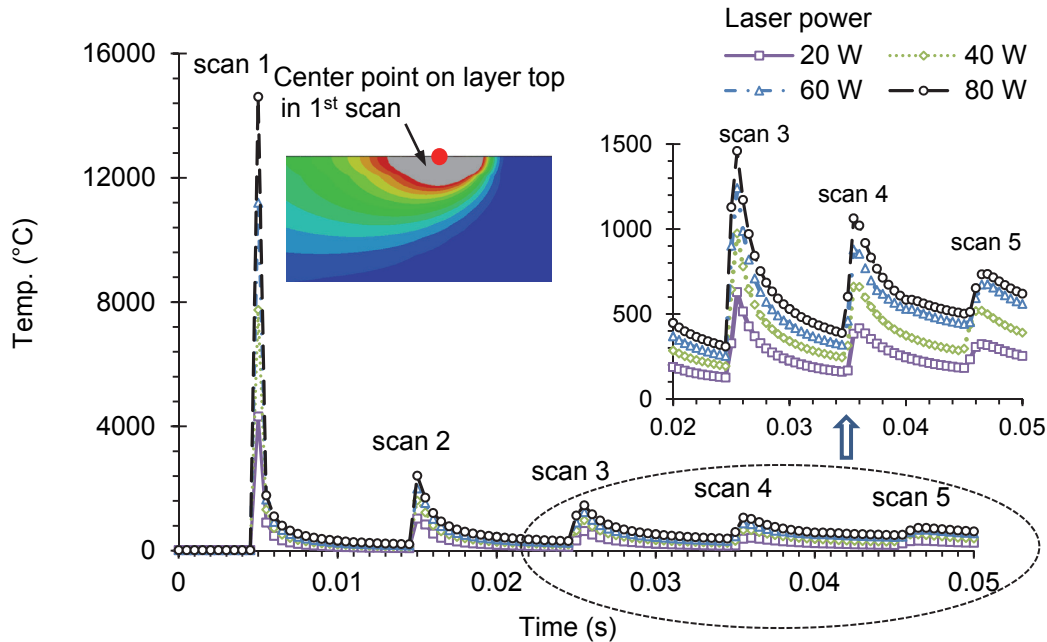
Fig. 13 Temperature history of center point on layer top in 1st scan.

3.3. Recommendation

The developed finite element model showed certain predictive capabilities. To improve the predictive accuracy, it is recommended that the absorptivity, specific heat, and thermal conductivity of the powder bed should be measured experimentally and used in simulation. Moreover, some other factors such as power loss, spot size, etc. should be considered in future research.

Another important factor that should be considered in the future is the computational time. More specifically, for each micro-scale simulation case in this study, the computational time was 240 hours with a standard desktop workstation. It is estimated that for a practical macro-scale selective laser melting part, the computational time would be a million year if the same mesh size is used, which is not practical. Therefore, it is critical to develop a scaling-up methodology from micro-scale level to macro-scale simulations without a significant cost of computational time. In this way, real parts with residual stress and distortion could be predicted.

4. Conclusions

This study focuses on the development of a novel simulation model for SLM. The effects of laser powder and material properties on molten pool geometry and temperature gradient were assessed. The predictions of molten pool geometry were verified by the experimental data. Key findings are summarized as follows:

- A new model of a physics-based layer build-up approach coupled with a surface moving heat flux was developed to simulate SLM.
- The molten pool geometries was predicted and verified by the experimental data with reasonable accuracy. It was predicted that balling will not occurs under the tested condition. It was also predicted that by using compact powders, the steep temperature gradient can be reduced and the molten pool size can be decreased.

1142

- The temperature gradient in the depth direction is much higher than those in width and laser scanning directions since the heat transfer in the depth direction is greatly constrained by the low thermal conductivity of the powder layers.
- The addition of subsequent layers significantly affected the temperature gradient and the melting of previous layers. It only takes few milliseconds to melt the material and cool it to room temperature, which indicated the very fast heating and cooling cycles in SLM.

Acknowledgement

References

[1]   Waterman, N.A., Dickens, P., 1994, "Rapid Product Development in the USA, Europe and Japan," World Class Design to Manufacture, 1(3), pp. 27-36.

[2]   Levy, G.N., Schindel, R., Kruth, J.P., 2003, "Rapid Manufacturing and Rapid Tooling with Layer Manufacturing (LM) Technologies, State of the Art and Future Perspectives," CIRP Annals - Manufacturing Technology, 52(2), pp. 589-609.

[3]   Guo, N., Leu, M., 2013, "Additive Manufacturing: Technology, Applications and Research Needs," Frontiers of Mechanical Engineering, 8(3), pp. 215-243.

[4]   Vandenbroucke, B., Kruth, J., 2007, "Selective Laser Melting of Biocompatible Metals for Rapid Manufacturing of Medical Parts," Rapid Prototyping Journal, 13(4), pp. 196-203.

[5]   Clare, A., Chalker, P., Davies, S., Sutcliffe, C., Tsopanos, S., 2008, "Selective Laser Melting of High Aspect Ratio 3D Nickel-Titanium Structures Two Way Trained for MEMS Applications," International Journal of Mechanics and Materials in Design, 4(2), pp. 181-187.

[6]   Hollander, D.A., von Walter, M., Wirtz, T., Sellei, R., Schmidt-Rohlfing, B., Paar, O., Erli, H., 2006, "Structural, Mechanical and in Vitro Characterization of Individually Structured Ti–6Al–4V Produced by Direct Laser Forming," Biomaterials, 27(7), pp. 955-963.

[7]   Rochus, P., Plesseria, J.-., Van Elsen, M., Kruth, J.-., Carrus, R., Dormal, T., 2007, "New Applications of Rapid Prototyping and Rapid Manufacturing (RP/RM) Technologies for Space Instrumentation," Acta Astronautica, 61(1–6), pp. 352-359.

[8]   Wong, M., Tsopanos, S., Sutcliffe, C., Owen, L., 2007, "Selective Laser Melting of Heat Transfer Devices," Rapid Prototyping Journal, 13(5), pp. 291-297.

[9]   Kruth, J.-., Levy, G., Klocke, F., Childs, T.H.C., 2007, "Consolidation Phenomena in Laser and Powder-Bed Based Layered Manufacturing," CIRP Annals - Manufacturing Technology, 56(2), pp. 730-759.

[10]   Yadroitsev, I., Gusarov, A., Yadroitsava, I., Smurov, I., 2010, "Single Track Formation in Selective Laser Melting of Metal Powders," Journal of Materials Processing Technology, 210(12), pp. 1624-1631.

[11]   Tolochko, N.K., Khlopkov, Y.V., Mozzharov, S.E., Ignatiev, M.B., Laoui, T., Titov, V.I., 2000, "Absorptance of Powder Materials Suitable for Laser Sintering," Rapid Prototyping Journal, 6(3), pp. 155-161.

[12]   Gusarov, A., Kovalev, E., 2009, "Model of Thermal Conductivity in Powder Beds," Physical Review B, 80(2), pp. 024202.

[13] Thijs, L., Verhaeghe, F., Craeghs, T., Humbeeck, J.V., Kruth, J., 2010, "A Study of the Microstructural Evolution during Selective Laser Melting of Ti–6Al–4V," Acta Materialia, 58(9), pp. 3303-3312.

[14] Roberts, I.A., Wang, C.J., Esterlein, R., Stanford, M., Mynors, D.J., 2009, "A Three-Dimensional Finite Element Analysis of the Temperature Field during Laser Melting of Metal Powders in Additive Layer Manufacturing," International Journal of Machine Tools and Manufacture, 49(12–13), pp. 916-923.

[15] Dong, L., Makradi, A., Ahzi, S., Remond, Y., 2009, "Three-Dimensional Transient Finite Element Analysis of the Selective Laser Sintering Process," Journal of Materials Processing Technology, 209(2), pp. 700-706.

[16] Hussein, A., Hao, L., Yan, C., Everson, R., 2013, "Finite Element Simulation of the Temperature and Stress Fields in Single Layers Built without-Support in Selective Laser Melting," Materials & Design, 52(0), pp. 638-647.

[17] Patil, R.B., Yadava, V., 2007, "Finite Element Analysis of Temperature Distribution in Single Metallic Powder Layer during Metal Laser Sintering," International Journal of Machine Tools and Manufacture, 47(7–8), pp. 1069-1080.

[18] Morsbach, C., Höges, S., Meiners, W., 2011, "Modeling the Selective Laser Melting of Polylactide Composite Materials," Journal of Laser Applications, 23(1), pp. 012005.

[19] Boivineau, M., Cagran, C., Doytier, D., Eyraud, V., Nadal, M., Wilthan, B., Pottlacher, G., 2006, "Thermophysical Properties of Solid and Liquid Ti-6Al-4V (TA6V) Alloy," International Journal of Thermophysics, 27(2), pp. 507-529.

[20] Ding, J., Colegrove, P., Mehnen, J., Ganguly, S., Sequeira Almeida, P.M., Wang, F., Williams, S., 2011, "Thermo-Mechanical Analysis of Wire and Arc Additive Layer Manufacturing Process on Large Multi-Layer Parts," Computational Materials Science, 50(12), pp. 3315-3322.

[21] Dai, K., Shaw, L., 2004, "Thermal and Mechanical Finite Element Modeling of Laser Forming from Metal and Ceramic Powders," Acta Materialia, 52(1), pp. 69-80.

[22] Verhaeghe, F., Craeghs, T., Heulens, J., Pandelaers, L., 2009, "A Pragmatic Model for Selective Laser Melting with Evaporation," Acta Materialia, 57(20), pp. 6006-6012.

[23] Boyer, R., Collings, E., 1993, "Materials properties handbook: Titanium alloys".

[24] Kruth, J.P., Froyen, L., Van Vaerenbergh, J., Mercelis, P., Rombouts, M., Lauwers, B., 2004, "Selective Laser Melting of Iron-Based Powder," Journal of Materials Processing Technology, 149(1–3), pp. 616-622.

[25] Dai, K., Shaw, L., 2002, "Distortion Minimization of Laser-Processed Components through Control of Laser Scanning Patterns," Rapid Prototyping Journal, 8(5), pp. 270-276.